RSC Advances

PAPER

View Article Online
View Journal | View Issue



Cite this: *RSC Adv.*, 2025, **15**, 19645

# Eco-friendly fabrication of sandwich-structured poly(imide-siloxane)/silver nanowire composite films for stretchable strain sensors†

Ye-Pin Son,‡[a] Daeho Choi,‡[b] Jaekang Lee,‡[b] Yun-Je Choi,[a] Seung-Won Jin,[a] Soohaeng Cho*[b] and Chan-Moon Chung *[a]

Polyimide (PI) films have gained significant recognition for aerospace, automotive, displays, microelectronics, and membrane applications due to their excellent mechanical and thermal properties and chemical resistance. However, conventional preparations of PI films have been performed using toxic organic solvents that are harmful to the environment and human health. In this work, stretchable PI films were first prepared using a green aqueous solvent for application as strain sensors. A poly(amic acid-siloxane) salt (PAASS) was synthesized using a solvent mixture (water and *tert*-butanol) from 3,3′,4,4′-biphenyltetracarboxylic dianhydride (BPDA), bis(3-aminopropyl)-terminated polydimethylsiloxane (PDMS), and *m*-phenylenediamine (MPD). The as-prepared aqueous PAASS solutions were drop-cast, and the resultant films were thermally imidized to obtain poly(imide-siloxane) (PIS) films. The films showed excellent elongation at break and 5% decomposition temperature (up to 436.7% and 466 °C, respectively). Stretchable strain sensors were fabricated in the form of sandwich-structured PIS/silver nanowire (AgNW)/PIS composite films. Preliminary strain sensor tests, including stretching/releasing cycles, demonstrated good GF values up to 28.4 and stable sensor performance over the strain range of 5–50% for the PIS/AgNW/PIS composite films. Our study provides an eco-friendly and economical fabrication method for stretchable PIS/AgNW/PIS composite strain sensors that have promising potential for next-generation stretchable device applications.

Received 26th February 2025
Accepted 3rd June 2025

DOI: 10.1039/d5ra01386k

rsc.li/rsc-advances



## 1. Introduction

Polyimides (PIs), high-performance engineering plastics, are widely used in various industries such as aerospace, automotives, displays, microelectronics, and membranes due to their excellent mechanical strength, thermal stability, and chemical resistance.[1–3] PIs are conventionally synthesized *via* poly(amic acid) (PAA) intermediates that are later chemically or thermally imidized.[4–6] PI synthesis has been performed traditionally using polar aprotic solvents such as *N*-methyl-2-pyrrolidone (NMP), *N*,*N*-dimethylacetamide (DMAc), and *N*,*N*-dimethylformamide (DMF), which are toxic organic solvents with high boiling points. As environmental regulations become stricter, efforts to reduce the use of these hazardous organic solvents have garnered significant attention.[7,8] Aqueous polymerization can address safety concerns for workers and minimize environmental impacts. Some studies in the polymer field have attempted to utilize water as a solvent in polymerization and processing.[9,10]

An eco-friendly synthesis method for PI *via* a poly(amic acid) salt (PAAS) intermediate has recently emerged. A PAAS is prepared from a dianhydride and a diamine in water in the presence of a tertiary amine such as pyridine, triethylamine, or 1,2-dimethylimidazole (DMIZ) *via* an acid–base reaction between the carboxyl group of PAA and the tertiary amine.[10–12] Due to its salt structure, a PAAS can be dissolved in green solvents such as water and ethanol and exhibits enhanced hydrolytic stability.[13,14] This is a simple, cost-effective, and environmentally sustainable approach that eliminates the need for harmful, expensive organic solvents. A few studies reported on eco-friendly PI synthesis using aqueous solvents and their applications. For example, environmentally friendly, low-temperature, solution-processed PI thin films with high hydrolytic stability were explored as gate dielectric layers for organic field-effect transistors.[14] A water-soluble PI precursor was synthesized using a facile one-step process for use as a Si anode binder in lithium-ion batteries.[15] An aqueous PAAS solution was prepared and used for application to thermally conductive PI films.[16] However, despite the timely importance of the green synthesis of PIs, published research on the

[a]*Department of Chemistry, Yonsei University, Wonju, Gangwon-do 26493, Republic of Korea. E-mail: cmchung@yonsei.ac.kr*

[b]*Department of Physics, Yonsei University, Wonju, Gangwon-do 26493, Republic of Korea. E-mail: shcho@yonsei.ac.kr*

† Electronic supplementary information (ESI) available. See DOI: https://doi.org/10.1039/d5ra01386k

‡ These authors contributed equally.

application of PIs prepared by an eco-friendly method is rare. In particular, there have been no reports on stretchable PIs prepared by an eco-friendly method.

Stretchable polymers have numerous applications, such as wearable electronics, stretchable batteries, soft robotics, flexible displays and strain sensors. Among the applications, stretchable strain sensors have received considerable attention in health monitoring, soft robotics, and electronic skin.[17–19] Strain sensors convert mechanical deformations into electrical signals, specifically through changes in resistance or capacitance. Polymer-based strain sensors, which are composed of elastomers and conductive inorganic fillers (*e.g.*, carbon black, carbon nanotubes, graphene, and silver nanowires (AgNWs)), have attracted interest due to their simple signal readout, straightforward fabrication process, and ability to detect various deformations such as torsion, bending, and stretching.[17–21] These features set them apart from traditional strain sensors based on rigid metals and inorganic semiconductors, which lack inherent flexibility.

This work presents the first stretchable PI copolymer films prepared using a green aqueous solvent for application as strain sensors. We provide an eco-friendly strategy for the preparation of poly(imide-siloxane) (PIS) films in a mixed solvent of distilled water and *tert*-butanol, which is regarded as a green solvent.[16,22] A poly(amic acid-siloxane) salt (PAASS) was prepared in the aqueous mixed solvent, and the resultant as-prepared solution was used to prepare PIS films. To find an optimum composition for practical applications in strain sensors, the PIS films were synthesized at various polydimethylsiloxane (PDMS) contents, and their thermal and mechanical properties were investigated. Finally, sandwich-structured PIS/AgNW/PIS composite films were fabricated by simple spray coating of an AgNW suspension in ethanol, embedding AgNW fillers between two PIS layers. The relative resistance variation under different levels of strain was measured to preliminarily examine the feasibility of the designed composite film as a resistive strain sensor.

## 2. Experimental section

### 2.1. Materials

3,3′,4,4′-Biphenyltetracarboxylic dianhydride (BPDA, 97%), *m*-phenylenediamine (MPD, 98%), and 1,2-dimethylimidazole (DMIZ, 97%) were purchased from Sigma-Aldrich (Seoul, Republic of Korea). Bis(3-aminopropyl)-terminated polydimethylsiloxane (PDMS, 99%, $\overline{M_w} = 850 - 900$ g mol$^{-1}$) was purchased from Gelest (Morrisville, USA). *tert*-Butanol (99.5%) was purchased from Daejung Chemicals (Seoul, Republic of Korea). A 1% ethanol suspension of silver nanowires (AgNW, 99.9%) with a diameter range of 20–40 nm and a length range of 10–20 μm was purchased from Ditto Technology (Gyeonggi-do, Republic of Korea). Silver paste was purchased from CANS (Tokyo, Japan). Distilled water was obtained using a purification system (PURELAB Option-Q, ELGA, UK).

### 2.2. Preparation of aqueous PAASS solutions and PIS films

PIS films were prepared *via* PAASS intermediates with varied compositions (Fig. 1 and Table 1). Below, we describe the preparation of PAASS-5, which has a molar ratio of BPDA, PDMS, and MPD of 1 : 0.7 : 0.3. For this, PDMS (16.30 g, 0.019 mol), MPD (0.86 g, 0.0080 mol), and DMIZ (7.68 g, 0.081 mol) were added to a mixed solvent containing distilled water (60.0 mL) and *tert*-butanol (51.2 mL). The mixture was stirred for 1 h under nitrogen. After the mixture was completely dissolved, BPDA (7.83 g, 0.027 mol) was added and reacted at 70 °C for 18 h to produce a PAASS-5 solution. A portion of the PAASS-5 solution was dried to obtain a PAASS-5 powder for FT-IR measurement and elemental analysis. The other PAASS samples were prepared by similar procedures.

The as-prepared PAASS solutions were drop-cast onto glass plates, and the resultant films were heated on a hot plate at 50 °C for 6 h to remove the solvent. The next step was a thermal imidization process involving stepwise heating of the films at 100 °C, 150 °C, 200 °C, and 250 °C, with each temperature maintained for 30 min. The films were then cooled to room temperature and peeled from the glass plates to obtain PIS films (Fig. S1†). To facilitate peeling, the coated glass plates were immersed in water and subjected to ultrasonication. The required ultrasonication time decreased with increasing PDMS content (Table S1†). The prepared PIS films had an average thickness of 0.14 mm and inherent viscosities ranging from 0.23 to 0.26 dL g$^{-1}$.

### 2.3. Fabrication of simple-structured and sandwich-structured composite films

Fig. S2a† schematically illustrates the fabrication of the strain sensor. The composite films were prepared with dimensions of 4 cm × 0.5 cm using PIS-5 films. Neither of the 0.5 cm-wide ends of a PIS film was coated to allow proper gripping, and silver paste was coated in areas of 0.5 × 0.5 cm$^2$ for the readout of electrical signals. To establish a conductive network, the AgNW suspension in ethanol was spray-coated onto a PIS-5 film (spraying pressure: 0.25 MPa) and dried at 150 °C for 3 min to obtain a simple-structured PIS/AgNW composite film. Next, the PAASS-5 solution was drop-cast onto the AgNW-deposited surface, and the solvent was evaporated at 50 °C for 6 h. Thermal imidization was performed at 100 °C, 150 °C, 200 °C, and 250 °C for 30 min each, affording a sandwich-structured PIS/AgNW/PIS composite film (Fig. S2b†). The sheet resistance of the simple-structured film was measured to be 43.1 Ω sq$^{-1}$ after eight spray coating cycles, and its conductivity was estimated at 121 600 S m$^{-1}$. The final sandwich-structured PIS/AgNW/PIS film had a thickness of 0.26 (±0.02) mm.

### 2.4. Characterization

To analyze the chemical structures of PAASSs, Fourier transform infrared (FT-IR) spectra were recorded using a Spectrum One B spectrometer (PerkinElmer, USA). For the PIS films, attenuated total reflectance (ATR) spectra were obtained using a Nicolet iS50 spectrometer (Thermo Fisher Scientific, USA). Inherent viscosity measurements were conducted at 30 °C using a Cannon-Fenske viscometer (Cannon Instrument Company, USA) at a concentration of 0.50 g dL$^{-1}$ in concentrated sulfuric acid. Elemental analysis (EA) for carbon (C), hydrogen (H), and

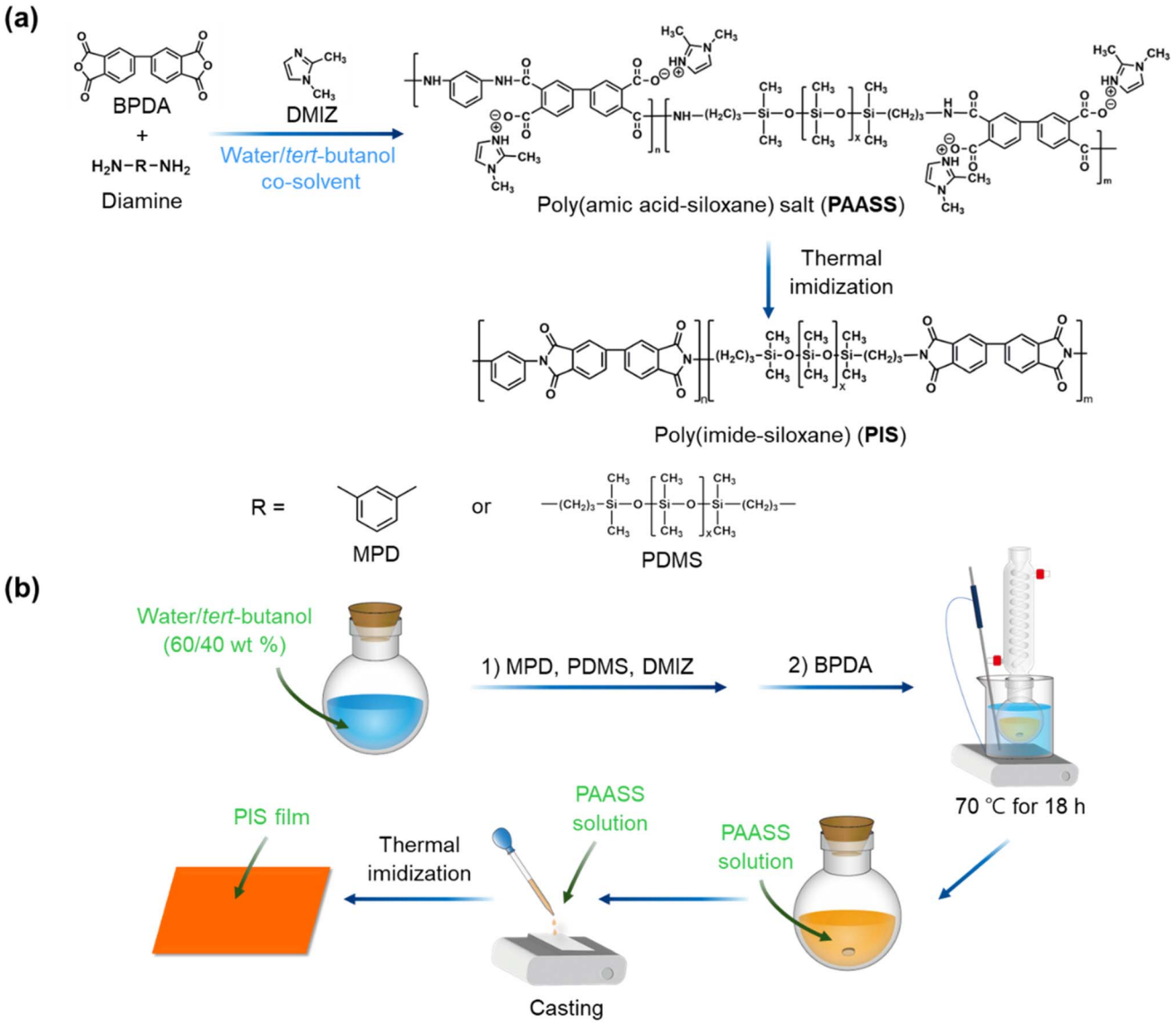


Fig. 1 (a) Synthetic route of PIS *via* a PAASS intermediate. (b) Schematic diagram showing the preparation of PIS films.

nitrogen (N) was performed using a FlashSmart elemental analyzer (Thermo Fisher Scientific, USA) to determine the compositions of PAASSs. Thermogravimetric analysis (TGA) was conducted to confirm the thermal stability of the PIS films. These measurements ranged from 50 °C to 800 °C at a heating rate of 10 °C $min^{-1}$ under nitrogen (Discovery TGA 55, TA Instruments, USA). Glass transition temperature measurements were performed using a DSC 25 (TA Instruments, Delaware,

Table 1 Composition of reagents for the synthesis of PIS[a]

| Sample code | Intermediate | DMIZ (g) | BPDA (g) | PDMS (g) | MPD (g) | PDMS/MPD mol ratio |
|---|---|---|---|---|---|---|
| PIS-1 | PAASS-1 | 11.40 | 11.63 | 10.38 | 2.99 | 0.4 (3/7) |
| PIS-2 | PAASS-2 | 10.17 | 10.37 | 12.34 | 2.29 | 0.7 (4/6) |
| PIS-3 | PAASS-3 | 9.18 | 9.36 | 13.92 | 1.72 | 1 (5/5) |
| PIS-4 | PAASS-4 | 8.36 | 8.53 | 15.22 | 1.25 | 1.5 (6/4) |
| PIS-5 | PAASS-5 | 7.68 | 7.83 | 16.30 | 0.86 | 2.3 (7/3) |
| PIS-6[b] | PAASS-6 | 7.10 | 7.24 | 17.23 | 0.53 | 4 (8/2) |

[a] The concentration of the combined BPDA, PDMS, and MPD in the mixed solvent was 20 wt%. [b] Under this composition of the reaction mixture, PIS could not be obtained due to the insolubility of PDMS in the mixed solvent.

USA) under a nitrogen flow of 50 mL $min^{-1}$ at a heating rate of 20 °C $min^{-1}$. The tensile strength and elongation at break of the PIS films were examined using a QC-505M1 (Daeha Trading, Republic of Korea) universal testing machine (UTM). The test specimens had a length of 60 mm and a width of 5 mm and were measured with a grip distance of 30 mm and a test speed of 100 mm $min^{-1}$. In addition, the tensile strength and elongation at break of each film were calculated as the average of five measurements. Field emission scanning electron microscopy (FE-SEM, JSM-7900F, Jeol, Japan) was utilized to examine the composite film cross-sections and surface morphologies at an acceleration voltage of 15 kV and a working distance of 10.0 mm. Mapping images of energy-dispersive X-ray spectroscopy (EDS) were obtained using an Aztec Live (Oxford Instruments, UK) to confirm that silicon (Si) was evenly distributed within the PIS films. The samples for strain sensing were prepared by AgNW suspension sprays using a BV-500T spray coating system (Banseok Precision, Republic of Korea), and sheet resistances of simple-structured PIS/AgNW composite films were calculated as the average of five measurements using a Hall effect measurement system (HMS-3000, Ecopia Company, Republic of Korea). For strain sensor performance, a test system was coupled with a linear stage module, MS-LSM-NK223-G1 (Motorbank, Republic of Korea), with grips and a Keithley 6514 multimeter (Keithley Instruments, USA) to record the *in situ* electrical signals under different tensile strains. To test the strain sensing characteristics, the two ends of the samples were fixed to motorized moving stages, and resistance measurements for all samples were recorded at a displacement rate of 0.5 mm $s^{-1}$ at room temperature. The gauge factor [$GF = (\Delta R/R_0)/\varepsilon$] values were calculated to determine the sensitivity of the composite films, where $R_0$ is their initial resistance without strain, $\Delta R$ is the resistance change under strain, $\varepsilon$ is the strain, and GF is the gauge factor.

## 3. Results and discussion

### 3.1. Preparation and characterization of stretchable PIS films

In this work, the PIS structure was employed to prepare a strain sensor matrix. The imide structure imparts mechanical strength and thermal stability, and the siloxane structure enhances stretchability. The preparation procedure of PIS films is shown in Fig. 1. For that, PDMS, MPD, and DMIZ were added to a mixed solvent of distilled water and *tert*-butanol (60 : 40 by mass) (Table 1). After complete dissolution, BPDA was added to the mixture, which was subsequently heated at 70 °C to prepare PAASS solution. Poly(amic acid-siloxane) structure was probably formed *via* reaction between BPDA and MPD and between BPDA and PDMS in the mixed solvent. The organic base DMIZ neutralizes the carboxyl group of poly(amic acid-siloxane) to form a carboxylate–ammonium salt, imparting water solubility to PAASS.[14] The synthesis of copolymers by incorporating MPD monomer can be conducive to film formation and also improve the mechanical properties of the film. When the molar ratio of PDMS/MPD was 8 : 2 or 9 : 1, the polymerization could not proceed because of the low solubility of PDMS in the mixed solvent. Therefore, polymerizations were conducted with molar ratios of PDMS/MPD of 3 : 7, 4 : 6, 5 : 5, 6 : 4, and 7 : 3. The optimum copolymer composition was determined based on the mechanical properties of the copolymers (see below). In this work, PDMS with a weight-average molecular weight ($\overline{M_w}$) of 850–900 g $mol^{-1}$ was employed because PDMS with a higher $\overline{M_w}$ of 3000 or 15 000 g $mol^{-1}$ was insoluble in the mixed solvent of distilled water and *tert*-butanol (60 : 40 by mass).

The reason for selecting the mass ratio (60 : 40) of distilled water to *tert*-butanol was that it enabled both successful PDMS dissolution and PAASS synthesis. *tert*-Butanol contains a hydroxyl group that is more efficiently shielded by alkyl groups than secondary and primary alcohols, which contributes to effective PDMS dissolution by minimizing the unfavorable interactions between the –OH groups and the PDMS hydrophobic groups.[23–25] In addition, *tert*-butanol is ranked as a 'recommended' green solvent with low toxicity and minimal environmental impact (including water, methanol, ethanol, *etc.*) based on publicly available solvent selection guides.[22]

The as-prepared aqueous PAASS solution was drop-cast onto a glass plate, and the resultant film was thermally imidized by stepwise heating up to 250 °C (Fig. 1b). The same procedure was repeated for the samples with molar ratios of PDMS/MPD of 3 : 7, 4 : 6, 5 : 5, 6 : 4, and 7 : 3 to prepare five PIS films (PIS-1, PIS-2,

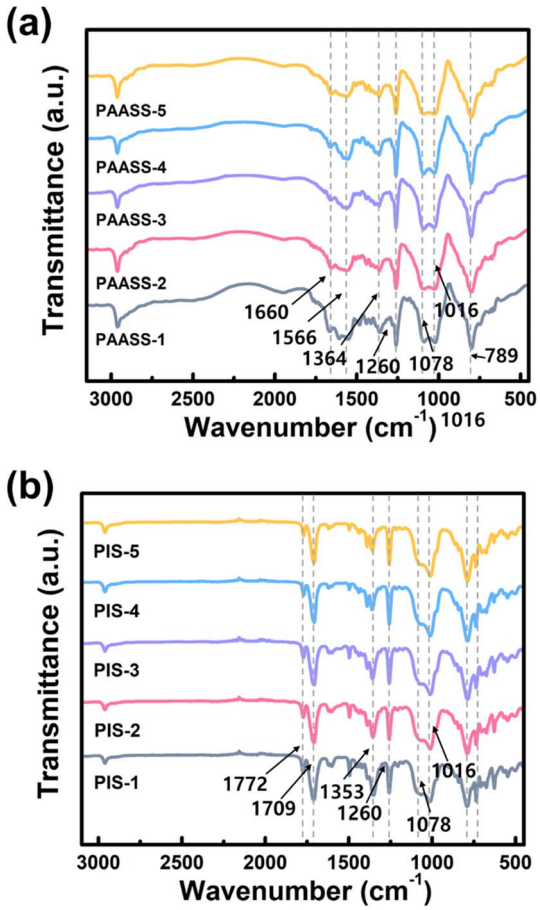


Fig. 2 FT-IR spectra of (a) PAASS and (b) PIS films.

PIS-3, PIS-4, and PIS-5, respectively). Fig. S1† shows images of the PIS-5 film with excellent stretchability and flexibility, allowing it to deform into various shapes without defects, which is important for wearability on human skin.

The chemical structures of PAASSs and PISs with various PDMS/MPD molar ratios were confirmed using FT-IR spectroscopy. As shown in Fig. 2a, the typical absorption bands of PAASS were observed at 1660 $cm^{-1}$ (amide C=O stretching), 1566 $cm^{-1}$ (carboxylate C=O asymmetric stretching), and 1364 $cm^{-1}$ (carboxylate C=O symmetric stretching). In addition, absorption bands attributable to the PDMS moieties in the PAASS copolymers were confirmed at 2960 $cm^{-1}$ (methyl $sp^3$ C–H stretching), 1260 $cm^{-1}$ (siloxane Si–C stretching), 1078 $cm^{-1}$ (siloxane Si–O asymmetric stretching), 1016 $cm^{-1}$ (siloxane Si–O symmetric stretching), and 789 $cm^{-1}$ (siloxane Si–C bending). Absorption bands related to the imide structure were not observed. The characteristic bands denote the formation of the salt structure and the incorporation of PDMS moieties into the backbone. Elemental analysis was performed on PAASS samples to confirm their compositions, which are summarized in Table S2.† The results of carbon (C), hydrogen (H), and nitrogen (N) are close to the corresponding theoretically calculated values. In Fig. 2b, the typical absorption bands of PISs appeared at 1772 $cm^{-1}$ (imide C=O asymmetric stretching), 1709 $cm^{-1}$ (imide C=O symmetric stretching), 1353 $cm^{-1}$ (imide C–N stretching), and 729 $cm^{-1}$ (imide C=O bending). In addition, absorption bands due to the PDMS moieties in the PISs were observed at 2960 $cm^{-1}$, 1260 $cm^{-1}$, 1078 $cm^{-1}$, 1016 $cm^{-1}$, and 789 $cm^{-1}$, which are identical to the corresponding wavenumbers for PAASS described above. These spectra imply that the PAASS underwent complete conversion to PIS *via* thermal imidization. Elemental analysis was also performed on PIS samples to confirm their structures and compositions, which are summarized in Table S3.† The results of carbon (C), hydrogen (H), and nitrogen (N) are almost identical to the corresponding theoretically calculated values. DMIZ is considered to have been completely removed because its boiling point (204 °C) is lower than the imidization temperature (250 °C), and the elemental analysis results support this. Molecular weights of PAASS and PIS could not measured by gel permeation chromatography (GPC) because they were not soluble in GPC solvents. Instead, the inherent viscosities of PISs were measured using sulfuric acid, which ranged from 0.23 to 0.26 dL $g^{-1}$.

The cross-sectional FE-SEM and corresponding EDS images of the PIS films with various PDMS/MPD molar ratios are presented in Fig. 3 and S3.† Phase separation may be expected in the PIS films because the imide structure has high rigidity and strong intermolecular forces, while siloxane structure has high flexibility and weak intermolecular forces.[26,27] If the PIS films were phase-separated, stable mechanical performance could not be obtained because of their phase inhomogeneity. The Fig. 3 and S3† show that silicon was uniformly distributed in the PIS films, indicating that phase separation of the PDMS structure did not occur. This uniformity probably arises because the PDMS used in this work had a short siloxane segment ($\overline{M_w}$ of PDMS = 850–900 g $mol^{-1}$) that is less likely to form phase-separated domains compared to a longer siloxane segment.[26,27]

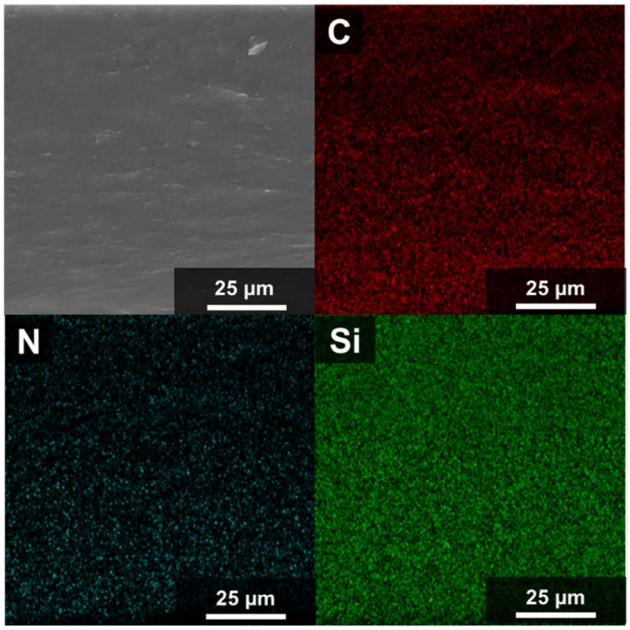


Fig. 3 Cross-sectional FE-SEM and EDS mapping images of a PIS-5 film.

### 3.2. Thermal and mechanical properties of PIS films

To examine the thermal stability of the PIS films, TGA curves were obtained (Fig. 4a and b and Table S4†). The $T_5$, $T_{10}$, and char yield values were derived from the curves and tended to slightly decrease as the PDMS content in the PIS film increased. This trend can be attributed to the reduced thermal stability with decreasing content of aromatic rings and imide groups within the copolymer chain. The PIS-5 film exhibited $T_5$, $T_{10}$, and char yield values (up to 800 °C) of 452 °C, 472 °C, and 13%, with less than 1% weight loss at temperatures up to approximately 400 °C. These results indicate that all of the PIS films demonstrate higher thermal stability relative to conventional strain sensor matrixes such as thermoplastic polyurethane (TPU) and polydimethylsiloxane matrix.[28,29] Glass transition temperatures of PISs were measured to be 124 °C or higher (Fig. S4 and Table S4†). The high thermal stability of PISs enables their potential applications in high-temperature strain sensing.

As shown in Fig. 4c and d, the mechanical properties of the PIS films were examined by stress–strain measurements, and the average values of the measurements are summarized in Table S5.† In the PIS-1 film, the tensile strength and elongation at break were 33.4 MPa and 57.4%, respectively. The elongation at break increased and tensile strength decreased with increasing PDMS content. The elongation at break of the PIS-5 film was 436.7%, which is comparable to those of conventional PIS films synthesized in organic solvents for stretchable device applications.[30,31] The maximized stretchability of the PIS-5 film results from the highest content of PDMS, which has

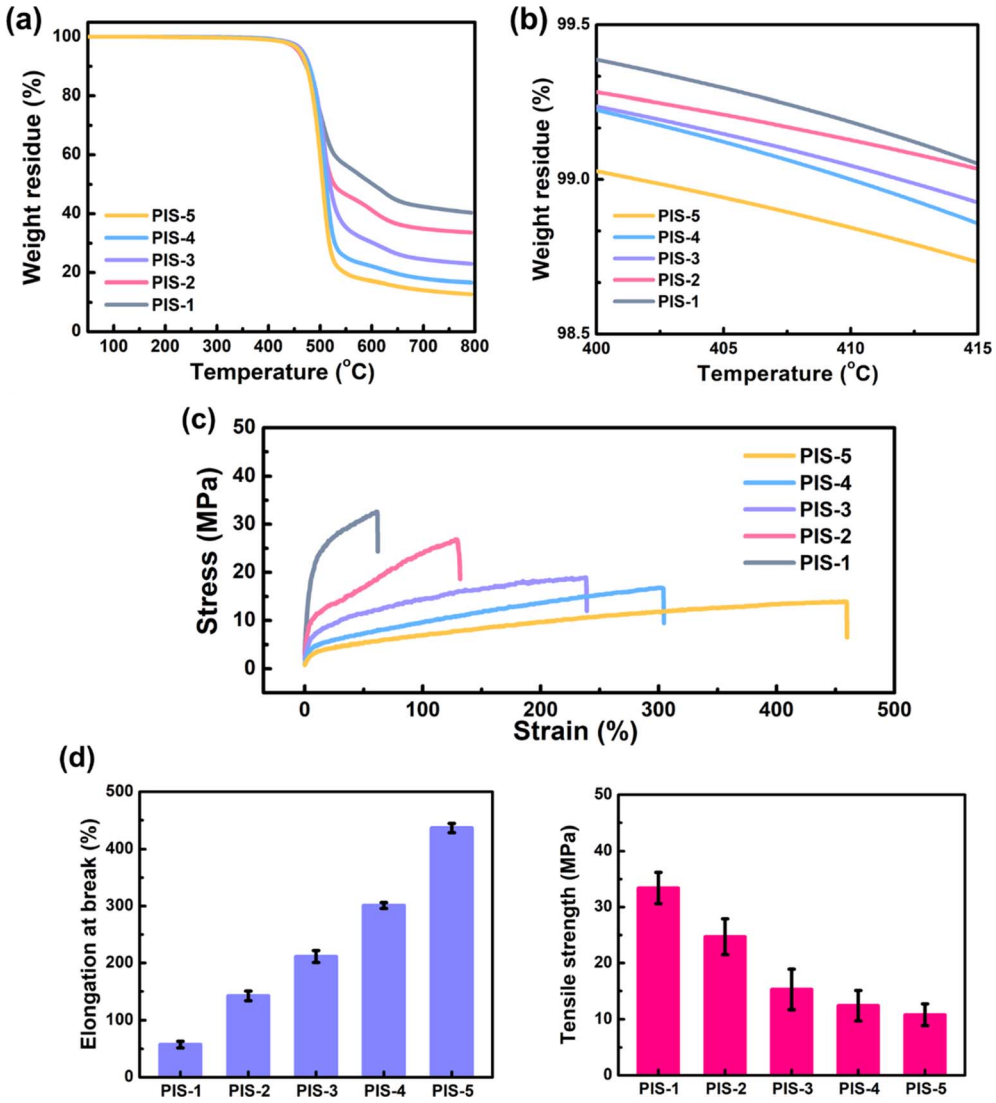


Fig. 4 (a and b) TGA curves, (c) stress–strain curves, and (d) elongation at break and tensile strength of PIS films.

a low rotation energy barrier and weak intermolecular interaction. The PIS-5 film, which exhibited good stretchability and appropriate tensile strength, was most suitable for application as strain sensors and were chosen as the matrix material of the strain sensor in this work.[32–34] An additional reason for selecting PIS-5 was its shortest ultrasonication time required for film peeling among the PIS samples (Table S1†).

### 3.3. Fabrication of sandwich-structured PIS/AgNW/PIS composite films for strain sensing

A dense and stable conductive network in the AgNW layer is required to output a consistent signal and for fabrication of the efficient strain sensor. The AgNW suspension in ethanol was sprayed onto one surface of PIS-5 film to ensure uniform distribution (Fig. S2a†). In the resulting simple-structured PIS/AgNW composite film, electrical current flows through the physical contact between the AgNWs. The sheet resistance of the simple-structured PIS/AgNW composite films was measured to determine the optimal number of sprays using the four-point probe method (Fig. S5 and Table S6†). The sheet resistance could not be detected after the 1st to 4th sprays because a conductive path was not generated but then rapidly decreased from 5 to 8 sprays, indicating the formation of a conductive network. The sheet resistance after the 8th spray was 43.1 Ω $sq^{-1}$, and no significant decrease in sheet resistance was observed with further sprays, indicating that a sufficient conductive network formed. Therefore, strain sensor tests were carried out using simple-structured and sandwich-structured composite films prepared by spraying with the AgNW suspension 8 times. The areal density of the simple-structured PIS/AgNW film increased with the number of spray coating cycles, reaching 2.0 μg $cm^{-2}$ after eight spray coatings (Fig. S5†).

The fabrication process of the sandwich-structured strain sensor is shown in Fig. S2a.† The PAASS-5 solution was drop-cast onto the AgNW side of the simple-structured PIS/AgNW composite film, followed by thermal imidization, to prepare

the sandwich-structured PIS/AgNW/PIS composite film (Fig. S2a and S2b†). The completely encapsulated structure prevents direct exposure of the AgNW layer to the external environment, mitigating the risk of permanent damage and deformation of the conductive network.

### 3.4. Morphological characterization

As shown in Fig. 5a and b of the simple-structured PIS/AgNW film, FE-SEM images revealed a highly uniform AgNW network across the surface of PIS-5 film, allowing consistent performance during sensor operation. Overall, the sprayed AgNWs overlapped each other without agglomeration on the film, forming a high-density random network. Dynamic changes in surface morphologies during the stretching/releasing cycles were observed on the simple-structured PIS/AgNW composite film under around 10% strain (Fig. 5c) due to the interaction between AgNWs and the PIS matrix under stress. The elastic modulus of AgNWs (81–176 GPa) is much higher than that of the PIS-5 matrix (2.48 MPa), and AgNWs and PIS-5 film can be considered rigid and flexible components, respectively.[35,36] During stretching, the overlapping AgNWs slide against each other due to the stiffness mismatch between the AgNWs and the polymer matrix.[19,20,37] After stretching, the surface morphology of the composite film was non-homogeneous at the microscale (Fig. 5c middle). In contrast, a homogeneous surface morphology was observed before stretching (Fig. 5c left). Some parts of the AgNW network fractured under the applied strain, while other parts retained their original structure (Fig. 5d). When the applied force was removed, the composite film returned to its original state (Fig. 5c right), and the rearranged AgNWs formed new conductive paths. This disconnection and reconnection of AgNWs induce changes in resistance, which explains the main working principle of the resistive strain sensor.[38–41]

### 3.5. Strain sensor characterization and preliminary response repeatability tests

To characterize the electromechanical behaviors of the simple-structured PIS/AgNW film and the sandwich-structured PIS/AgNW/PIS composite film, each film was attached to a motorized moving stage (Fig. S6†) and subjected to stretching and releasing cycles. The behavior of the simple-structured PIS/AgNW composite film under stretching/releasing cycles was investigated by experimental pre-test, as shown in Fig. S7a.† The simple-structured composite film indicated a large relative resistance variation ($\Delta R/R_0$) under 10% strain and its initial resistance value could not be recovered. It is considered that the exposed surface of the simple-structured composite film

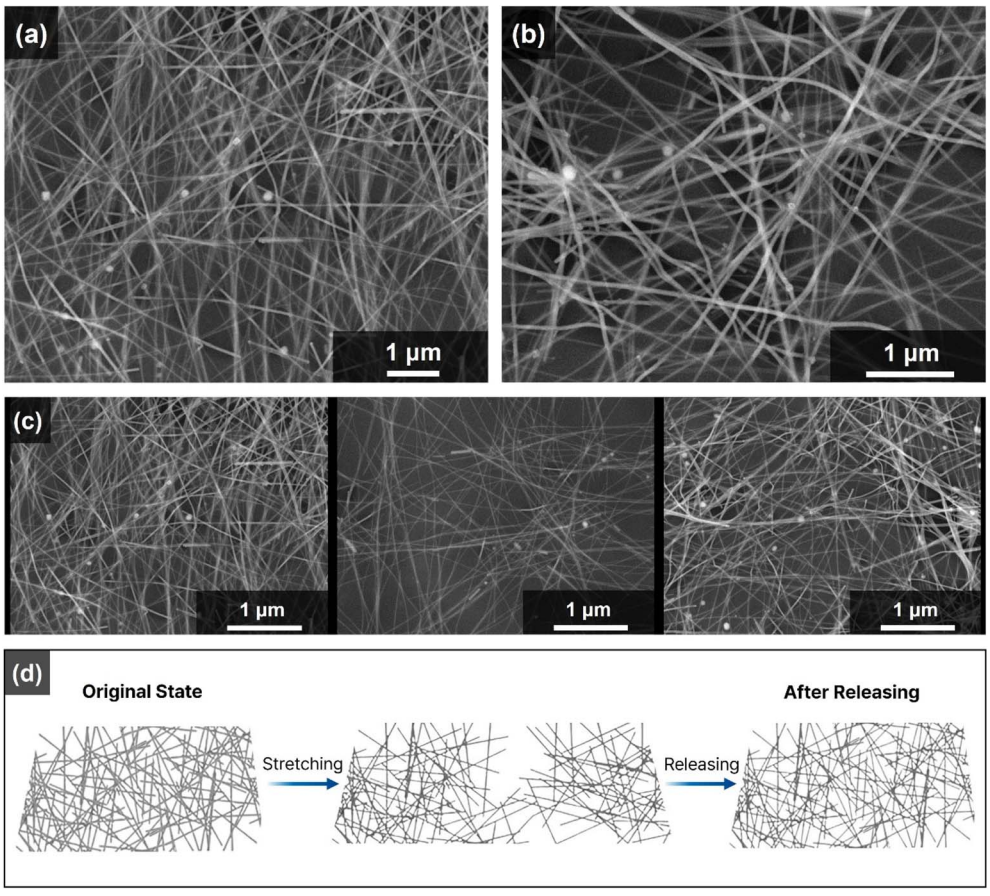


Fig. 5 FE-SEM images of the simple-structured PIS/AgNW composite film surfaces at (a) 150 00× and (b) 250 00× magnification. (c) FE-SEM images of surface morphology for the simple-structured films before stretching (left), under a strain of *ca.* 10% (middle), and after releasing (right). (d) Illustration of AgNW conductive paths upon stretching/releasing.

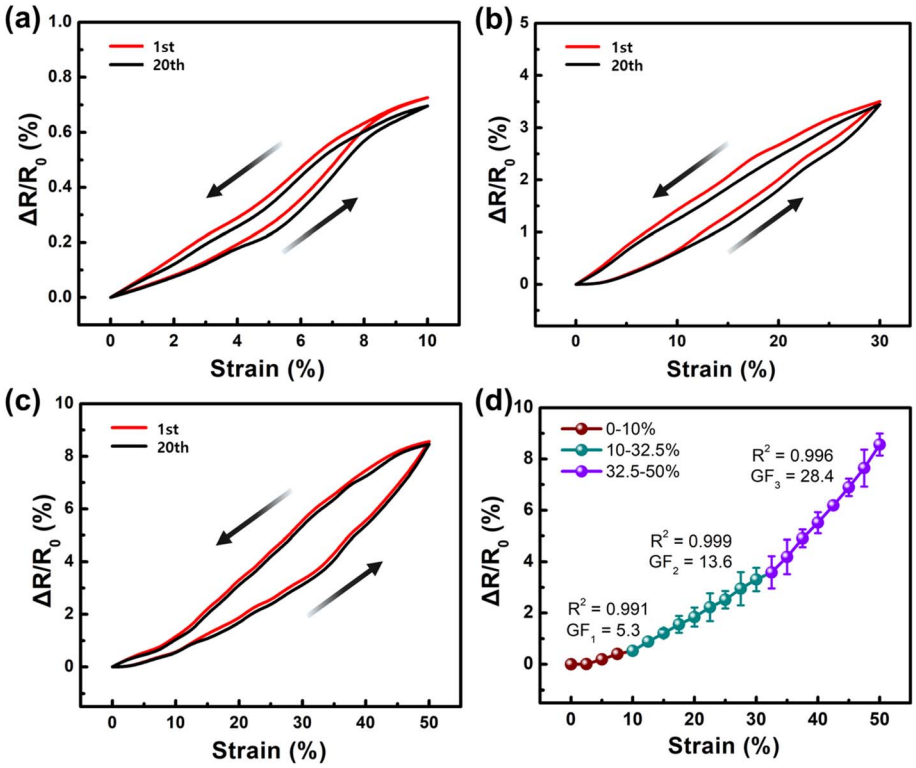


Fig. 6 Relative resistance variations ($\Delta R/R_0$) of the sandwich-structured PIS/AgNW/PIS composite films under (a) 10%, (b) 30%, and (c) 50% strain during the first and the 20th stretching/releasing cycles. (d) The $\Delta R/R_0$ of the sandwich-structured films *versus* the applied strain up to 50% and the corresponding gauge factors.

underwent buckling or fracture of the AgNW network, irreversibly increasing the electrical resistance.[40,42] On the other hand, in the sandwich-structured PIS/AgNW/PIS composite film, AgNWs were completely embedded to prevent permanent destruction, resulting in a stable response (Fig. S7b†). Therefore, the sandwich-structured composite films were used in further strain tests to investigate sensor performance.

Hysteresis with different output values during a stretching/releasing cycle was observed under 10%, 30%, and 50% strains in the sandwich-structured composite film (Fig. 6a–c).

Table 2 Comparison of AgNW/polymer composite strain sensors reported previously

| Polymer | Fabrication method | Max. gauge factor | Stretchability (%) | Response time (ms) | Durability (no. of cycles) | Ref. no. |
|---|---|---|---|---|---|---|
| PDMS | Drop casting | 14 | 70 | 87 | 1000 | 40 |
| PDMS | Dip coating | 89.99 | 60 | <800 | 1000 | 43 |
| PDMS | Spin coating | 30 | 100 | 100–200 | 2500 | 44 |
| PDMS | Dip coating<br>Spin coating<br>Contact transfer printing | 41.1 | 35 | 100–300 | 1000 | 45 |
| PDMS | Laser cutting<br>Drop coating | 846 | 150 | 100–200 | 1000 | 46 |
| PDMS | Vacuum filtration and transfer | 20 | 35 | 100–200 | 1000 | 47 |
| PDMS | Drop casting | 536.98 | 9 | 300–500 | — | 48 |
| TPU/PDMS[a] | Electro-spinning<br>Vacuum filtration<br>Spin coating | 12.9 | 50 | 200–400 | 1600 | 49 |
| TPU[a] | Casting | 6.78 | 372 | 300 | — | 50 |
| PU[b] | Spray coating<br>Plasma treatment | 11.2 | 500 | 200 | 5000 | 51 |
| PVA[c] | Freezing thawing | 0.58 | 500 | 320 | 2000 | 52 |
| Ecoflex[d] | Inkjet printing | 2.2 | 30 | 500–600 | 1000 | 53 |
| PIS | Drop casting spray coating | 28.4 | 50 | 600 | 1000 | This work |

[a] Thermoplastic polyurethane. [b] Polyurethane. [c] Poly(vinyl alcohol). [d] Commercial product.

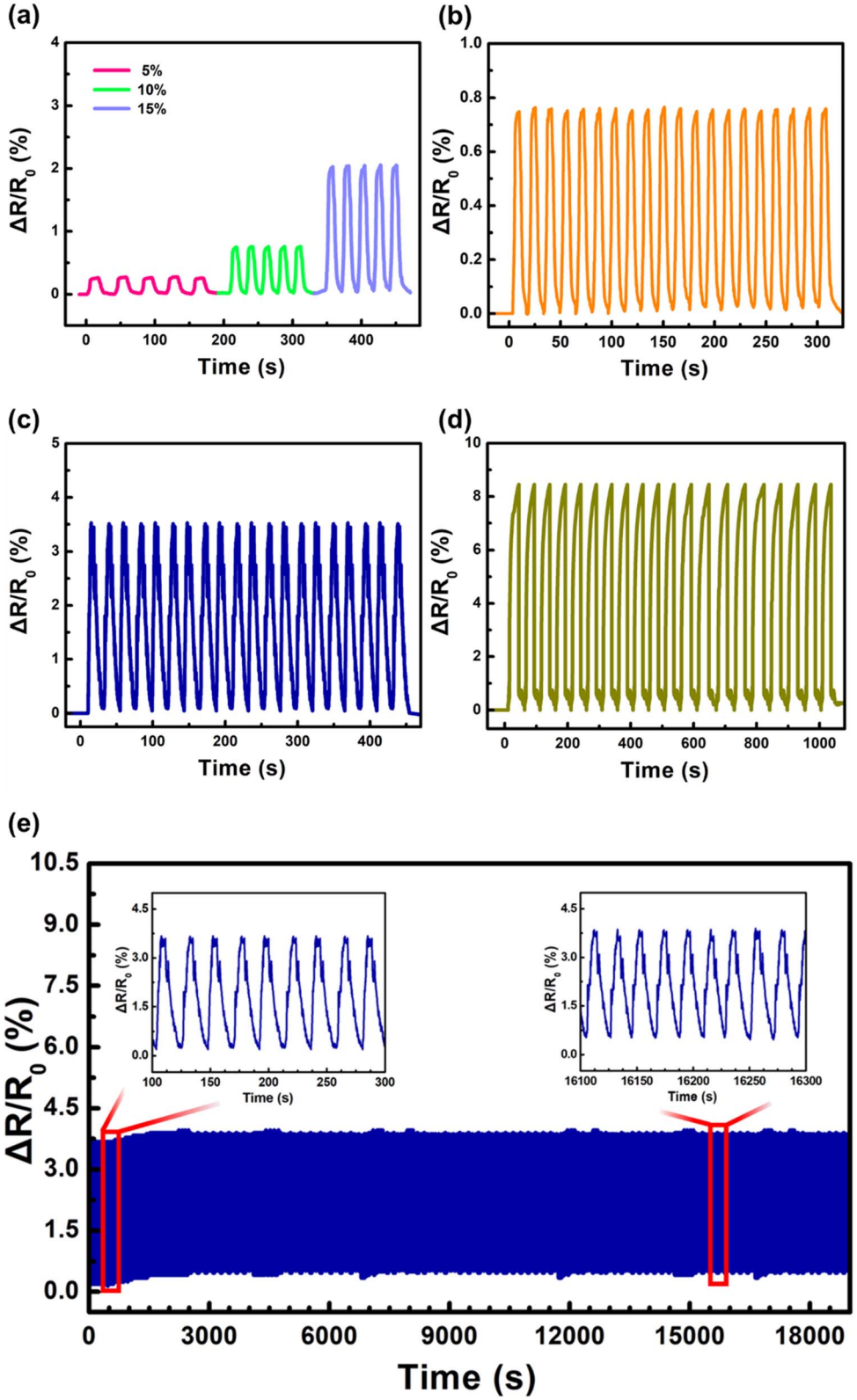


Fig. 7 (a) Relative resistance variation ($\Delta R/R_0$) of the sandwich-structured PIS/AgNW/PIS composite films *versus* time with a stepwise increase in strain from 5% to 15%. Response of the sandwich-structured films under (b) 10%, (c) 30%, (d) 50% strain during 20 stretching/releasing cycles, and (e) 30% strain during 1000 stretching/releasing cycles.

The reason for the hysteresis is that the uniformly arranged AgNW network in the film changes into an irregular network during deformation, leading to a bottleneck phenomenon that restricts current flow (Fig. 5d).[40] This bottleneck causes a nonlinear change in current over time, inducing hysteresis behavior. With increasing strain from 10% to 50%, both the hysteresis responses and the $\Delta R/R_0$ values increased. Fig. 6a–c show that, under each strain condition, the PIS/AgNW/PIS sample exhibits relatively similar hysteresis behavior in the first and the 20th stretching/releasing cycles. This result indicates that the hysteresis curves converged to a consistent shape without significant changes between 1 and 20 cycles, suggesting that the hysteresis of the strain sensor has reached a saturated state. Furthermore, under each strain condition, the $\Delta R/R_0$ values remain nearly the same in both the first and the 20th cycles. Fig. 6d presents the GF values and workable ranges with three relatively linear curve parts of 0–10%, 10–32.5%, and 32.5–50%, with GF values of 5.3, 13.6, and 28.4, respectively. As summarized in Table 2, the reported GF values in the literature on AgNW/polymer-based strain sensors generally range from 0.58 to 89.99, with a few reported extraordinary values (537–846). The three linear regions for the relative resistance change with increasing strain may be caused by stepwise destruction of the AgNW network. When the sensor was under strain of 0–10%, slight slippage between the AgNWs occurred and the resistance slightly increased. With a further strain increase up to 10–32.5%, some AgNWs started to be separated from each other, resulting in larger increase in the resistance. When the sensor was strained up to 32.5–50%, the AgNW network was largely fractured (Fig. 5d), more sharp increase in the resistance occurred. The reported stretchability and response time have ranges of 9–500% and 87–800 ms, respectively (Table 2). Our composite film has the advantage of being fabricated through a relatively simple process while exhibiting relatively good strain sensor performance (Table 2).

Repeated stretching/releasing cycles were applied to the sandwich-structured composite films to evaluate the response repeatability and durability of the strain sensors. As shown in Fig. 7a, the films exhibited stable and discernible detection patterns within the strain range of 5% to 15%. This can be attributed to the robust interfacial adhesion between the AgNWs and the PIS matrix in the sandwich-structured composite film, where the AgNW network remains tightly trapped in the polymer matrix. Furthermore, the films output stable electrical signals under 10%, 30%, and 50% strain over 20 stretching/releasing cycles (Fig. 7b–d). The long-term durability of the sandwich-structure composite films was verified under 30% strain for 1000 stretching/releasing cycles, showing steady performance and a negligible increase in resistance (Fig. 7e). These results suggest that sandwich-structured PIS/AgNW/PIS composite films have high electromechanical stability and hold great potential for applications as strain sensors. The PIS/AgNW/PIS sensor showed more stable 1000-cycle response repeatability under 30% strain than under 50% strain. For improved electromechanical stability of the strain sensor, further fine-tuning of the polymer composition and fabrication process are required.

# 4. Conclusions

PIS films were successfully prepared using a green solvent (water and *tert*-butanol mixture) *via* an eco-friendly PIS synthesis and film casting strategy that avoids the use of harmful organic solvents. The PIS-5 film exhibited excellent elongation at break and appropriate tensile strength (436.7 $\pm$ 7.9% and 10.8 $\pm$ 1.9 MPa, respectively) due to integration of the siloxane moiety into the PI backbone. These mechanical properties are comparable to those of other PIS films that were conventionally synthesized in organic solvents. The PIS films dramatically enhanced thermal stability, with $T_5$ greater than 450 °C, relative to conventional strain sensor substrates such as TPU and PDMS. The AgNW suspension was sprayed onto PIS substrate and then drop-cast with additional PIS solution to afford the sandwich-structured PIS/AgNW/PIS composite film as a resistive strain sensor. The formation of an efficient conductive path was demonstrated by FE-SEM, and the strain sensor showed good GF values up to 28.4, which are comparable to the reported GF values in the literature on polymer substrate/AgNW-based strain sensors. The preliminary response repeatability tests of the PIS/AgNW/PIS sensor showed stable sensor performance over the strain range of 5–50%. Our PIS/AgNW/PIS composite film demonstrates significant promise for future strain sensor applications.

# Data availability

All the data for the manuscript is available in the manuscript.

# Author contributions

Ye-Pin Son: conceptualization, investigation, formal analysis, data curation, writing – original draft. Daeho Choi: conceptualization, investigation, formal analysis, data curation. Jaekang Lee: investigation, formal analysis, data curation. Yun-Je Choi: data curation. Seung-Won Jin – data curation. Soohaeng Cho: supervision, writing – review & editing. Chan-Moon Chung: supervision, writing – review & editing.

# Conflicts of interest

The authors declare that they have no known competing financial interests or personal relationships that could have appeared to influence the work reported in this article.

# Acknowledgements

This work was supported by the Technology Innovation Program (20010315) funded by the Ministry of Trade, Industry, and Energy (MOTIE, Korea).

# References

1 Y. Li, G. Sun, Y. Zhou, G. Liu, J. Wang and S. Han, *Prog. Org. Coat.*, 2022, **172**, 107103.

2 P. Ma, C. Dai, H. Wang, Z. Li, H. Liu, W. Li and C. Yang, *Compos. Commun.*, 2019, **16**, 84–93.
3 Z. Xu, Z. L. Croft, D. Guo, K. Cao and G. Liu, *J. Polym. Sci.*, 2021, **59**, 943–962.
4 W. Chen, W. Chen, B. Zhang, S. Yang and C. Y. Liu, *Polymer*, 2017, **109**, 205–215.
5 D. J. Liaw, K. L. Wang, Y. C. Huang, K. R. Lee, J. Y. Lai and C. S. Ha, *Prog. Polym. Sci.*, 2012, **37**, 907–974.
6 C. Sroog, Polyimides, *Prog. Polym. Sci.*, 1991, **16**, 561–694.
7 T. Erdmenger, C. Guerrero-Sanchez, J. Vitz, R. Hoogenboom and U. S. Schubert, *Chem. Soc. Rev.*, 2010, **39**, 3317–3333.
8 D. Zou, S. P. Nunes, I. F. Vankelecom, A. Figoli and Y. M. Lee, *Green Chem.*, 2021, **23**, 9815–9843.
9 L. V. Kayser, M. D. Russell, D. Rodriquez, S. N. Abuhamdieh, C. Dhong, S. Khan, A. N. Stein, J. Ramírez and D. J. Lipomi, *Chem. Mater.*, 2018, **30**, 4459–4468.
10 S. Zheng, L. Jiang, C. Zhang, N. Ma and X. Liu, *Polym. Chem.*, 2022, **13**, 2375–2382.
11 H. Zhou, S. Zheng, C. Qu, D. Wang, C. Liu, Y. Wang, X. Fan, W. Xiao, H. Li and D. Zhao, *Eur. Polym. J.*, 2019, **114**, 346–352.
12 Y. So, J. Park, Y. M. Ha, J. Kim, N. K. Park, Y. Y. Kang, W. Lee, S. Lee, S. J. Oh and S. J. Kwak, *ACS Sustain. Chem. Eng.*, 2024, **12**, 14747–14759.
13 D. Cai, J. Su, M. Huang, Y. Liu, J. Wang and L. Dai, *Polym. Degrad. Stab.*, 2011, **96**, 2174–2180.
14 Y. Jeong, H. Park, Y. So, H. J. Mun, T. J. Shin, N. K. Park, J. Kim, S. Yoo, J. C. Won and Y. H. Kim, *J. Mater. Chem. C*, 2020, **8**, 14370–14377.
15 Y. So, H. S. Bae, Y. Y. Kang, J. Y. Chung, N. K. Park, J. Kim, H. T. Jung, J. C. Won, M. H. Ryou and Y. H. Kim, *Nanomaterials*, 2021, **11**, 3164.
16 S.-W. Jin, Y.-J. Jin, Y.-P. Son, Y.-J. Choi, J.-H. Ko, C.-H. Park, Y.-J. Jang and C.-M. Chung, *Compos. Commun.*, 2024, **48**, 101918.
17 H. Souri, H. Banerjee, A. Jusufi, N. Radacsi, A. A. Stokes, I. Park, M. Sitti and M. Amjadi, *Adv. Intell. Syst.*, 2020, **2**, 2000039.
18 T. Yang, D. Xie, Z. Li and H. Zhu, *Mater. Sci. Eng. R Rep.*, 2017, **115**, 1–37.
19 M. Amjadi, K. U. Kyung, I. Park and M. Sitti, *Adv. Funct. Mater.*, 2016, **26**, 1678–1698.
20 J. Chen, Q. Yu, X. Cui, M. Dong, J. Zhang, C. Wang, J. Fan, Y. Zhu and Z. Guo, *J. Mater. Chem. C*, 2019, **7**, 11710–11730.
21 F. Han, M. Li, H. Ye and G. Zhang, *Nanomaterials*, 2021, **11**, 1220.
22 D. Prat, A. Wells, J. Hayler, H. Sneddon, C. R. McElroy, S. Abou-Shehada and P. J. Dunn, *Green Chem.*, 2016, **18**, 288–296.
23 G. Cocchi, M. G. De Angelis and F. Doghieri, *J. Membr. Sci.*, 2015, **492**, 600–611.
24 J. H. Koschwanez, R. H. Carlson and D. R. Meldrum, *PLoS One*, 2009, **4**, e4572.
25 J. N. Lee, C. Park and G. M. Whitesides, *Anal. Chem.*, 2003, **75**, 6544–6554.
26 C. M. Mahoney, J. A. Gardella and J. C. Rosenfeld, *Macromolecules*, 2002, **35**, 5256–5266.
27 A. Tiwari, R. Sugamoto and L. H. Hihara, *Prog. Org. Coat.*, 2006, **57**, 259–272.
28 B. Masiulanis, *J. Appl. Polym. Sci.*, 1984, **29**, 681–690.
29 R. N. Santra, P. Mukunda, G. Nando and T. Chaki, *Thermochim. Acta*, 1993, **219**, 283–292.
30 L. C. Hsu, C. C. Shih, H. C. Hsieh, Y. C. Chiang, P. H. Wu, C. C. Chueh and W. C. Chen, *Polym. Chem.*, 2018, **9**, 5145–5154.
31 L. C. Hsu, Y. C. Lin, C. K. Chen, W. C. Yang, J. C. Ho and W. C. Chen, *ACS Appl. Polym. Mater.*, 2022, **4**, 3498–3510.
32 L. Huang, X. Huang, X. Bu, S. Wang and P. Zhang, *Sens. Actuators, A*, 2023, **359**, 114508.
33 X. Li, S. Xiao, Y. Lao, D. Li, Q. Wei, L. Ye and S. Lu, *Int. J. Biol. Macromol.*, 2024, **266**, 131004.
34 J. Lan, Y. Li, B. Yan, C. Yin, R. Ran and L. Y. Shi, *ACS Appl. Mater. Interfaces*, 2020, **12**, 37597–37606.
35 X. Li, H. Gao, C. J. Murphy and K. Caswell, *Nano Lett.*, 2003, **3**, 1495–1498.
36 B. Wu, A. Heidelberg, J. J. Boland, J. E. Sader, X. Sun and Y. Li, *Nano Lett.*, 2006, **6**, 468–472.
37 Alamusi, N. Hu, H. Fukunaga, S. Atobe, Y. Liu and J. Li, *Sensors*, 2011, **11**, 10691–10723.
38 Y. Lu, M. C. Biswas, Z. Guo, J. W. Jeon and E. K. Wujcik, *Biosens. Bioelectron.*, 2019, **123**, 167–177.
39 H. Liu, Q. Li, S. Zhang, R. Yin, X. Liu, Y. He, K. Dai, C. Shan, J. Guo and C. Liu, *J. Mater. Chem. C*, 2018, **6**, 12121–12141.
40 M. Amjadi, A. Pichitpajongkit, S. Lee, S. Ryu and I. Park, *ACS Nano*, 2014, **8**, 5154–5163.
41 Y. Zheng, Y. Li, K. Dai, Y. Wang, G. Zheng, C. Liu and C. Shen, *Compos. Sci. Technol.*, 2018, **156**, 276–286.
42 F. Xu and Y. Zhu, *Adv. Mater.*, 2012, **24**, 5117–5122.
43 J. H. Choi, M. G. Shin, Y. Jung, D. H. Kim and J. S. Ko, *Micromachines*, 2020, **11**, 156.
44 C. J. Lee, K. H. Park, C. J. Han, M. S. Oh, B. You, Y. S. Kim and J. W. Kim, *Sci. Rep.*, 2017, **7**, 1–8.
45 J. H. Cho, S.-H. Ha and J.-M. Kim, *Nanotechnology*, 2018, **29**, 155501.
46 Z. Wang, L. Zhang, J. Liu and C. Li, *ACS Appl. Mater. Interfaces*, 2019, **11**, 5316–5324.
47 X. Liao, Z. Zhang, Z. Kang, F. Gao, Q. Liao and Y. Zhang, *Mater. Horiz.*, 2017, **4**, 502–510.
48 Y. Du, Q. Zhang, K. Zhuo, J. Ji, Z. Yuan, C. Ji, W. Zhang and S. Sang, *Nano-Micro Lett.*, 2019, **14**, 168–172.
49 L. Lu, X. Wei, Y. Zhang, G. Zheng, K. Dai, C. Liu and C. Shen, *J. Mater. Chem. C*, 2017, **5**, 7035–7042.
50 P. Hashemi, M. Mehranpour and I. Ghasemi, *Polym. Compos.*, 2021, **42**, 1440–1450.
51 Y. X. Song, W. M. Xu, M. Z. Rong and M. Q. Zhang, *J. Mater. Chem. A*, 2019, **7**, 2315–2325.
52 S. Azadi, S. Peng, S. A. Moshizi, M. Asadnia, J. Xu, I. Park, C. H. Wang and S. Wu, *Adv. Sci. Technol.*, 2020, **5**, 2000426.
53 R. Madhavan, *J. Mater. Sci.: Mater. Electron.*, 2022, **33**, 3465–3484.